Environmental Science & Technology

Article

pubs.acs.org/est

# Visualizing Organophosphate Precipitation at the Calcite–Water Interface by in Situ Atomic-Force Microscopy

Lijun Wang,[*,†] Lihong Qin,[†] Christine V. Putnis,[*,‡,#] Encarnación Ruiz-Agudo,[§] Helen E. King,[∥] and Andrew Putnis[‡,⊥]

[†]College of Resources and Environment, Huazhong Agricultural University, Wuhan 430070, China

[‡]Institut für Mineralogie, University of Münster, 48149 Münster, Germany

[#]Nanochemistry Research Institute, Department of Chemistry, Curtin University, Perth, Western Australia 6845, Australia

[§]Department of Mineralogy and Petrology, University of Granada, Fuentenueva s/n, Granada 18071, Spain

[∥]Department of Earth Sciences, Utrecht University, 3584 CD Utrecht, The Netherlands

[⊥]The Institute for Geoscience Research (TIGeR), Curtin University, Perth, Western Australia 6102, Australia

Supporting Information

**ABSTRACT:** Esters of phosphoric acid constitute a large fraction of the total organic phosphorus (OP) in the soil environment and, thus, play an important role in the global phosphorus cycle. These esters, such as glucose-6-phosphate (G6P), exhibit unusual reactivity toward various mineral particles in soils, especially those containing calcite. Many important processes of OP transformation, including adsorption, hydrolysis, and precipitation, occur primarily at mineral–fluid interfaces, which ultimately governs the fate of organophosphates in the environment. However, little is known about the kinetics of specific mineral-surface-induced adsorption and precipitation of organophosphates. Here, by using in situ atomic-force microscopy (AFM) to visualize the dissolution of calcite $(10\bar{1}4)$ faces, we show that the presence of G6P results in morphology changes of etch pits from the typical rhombohedral to a fan-shaped form. This can be explained by a site-selective mechanism of G6P–calcite surface interactions that stabilize the energetically unfavorable (0001) or (0112) faces through step-specific adsorption of G6P. Continuous dissolution at calcite $(10\bar{1}4)$–water interfaces caused a boundary layer at the calcite–water interface to become supersaturated with respect to a G6P–Ca phase that then drives the nucleation and growth of a G6P–Ca precipitate. Furthermore, after the introduction of the enzyme alkaline phosphatase (AP), the precipitates were observed to contain a mixture of components associated with G6P–Ca, amorphous calcium phosphate (ACP)–hydroxyapatite (HAP) and dicalcium phosphate dihydrate (DCPD). These direct dynamic observations of the transformation of adsorption- and complexation-surface precipitation and enzyme-mediated pathways may improve the mechanistic understanding of the mineral-interface-induced organophosphate sequestration in the soil environment.

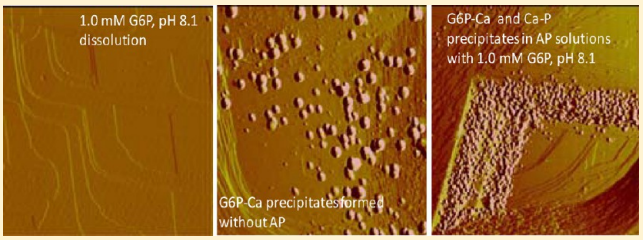


## INTRODUCTION

In soils, sediments, and waters, the organic phosphorus (OP) fraction, which includes nucleic acids, phospholipids, inositol phosphates (IP), sugar phosphates, phosphoproteins, and phosphonates, is at least as abundant as inorganic phosphorus (P).[1,2] In some environments, these can constitute as much as 80% of the total P pool.[3] These OP, such as IP,[4] can easily enter water bodies through leaching and runoff after hydrolysis of the ester bond.[5] This will increase the environmental risk of eutrophication.[6] The hydrolysis of OP can be mediated by extracellular phosphatases and phytases,[7−9] or occur abiotically on some mineral surfaces.[10]

OP such as IP and sugar phosphates can be strongly adsorbed onto iron and aluminum oxides in acidic soils or calcite in alkaline soils.[11−13] Moreover, proteins and enzymes can also adsorb onto mineral surfaces,[14,15] where the enzyme-driven interfacial hydrolysis and transformation pathway for the breakdown of organic P is different from that in bulk solutions. Following adsorption, precipitation of calcium salts has been proposed as a mechanism in IP retention on calcite,[13] suggesting that calcite surfaces act as concentrators of organophosphates through cation binding prior to precipitation.

Although these results have suggested that the surface precipitation process involves the dissolution of calcite, direct imaging of the kinetic pathways of nucleation and growth of OP precipitation has not been yet reported; thus, the precise role of mineral–water interfaces in controlling the rates of OP precipitation in the absence and presence of enzymes is still not

Received: October 22, 2015
Revised: December 3, 2015
Accepted: December 4, 2015
Published: December 4, 2015





DOI: 10.1021/acs.est.5b05214
Environ. Sci. Technol. 2016, 50, 259−268

well understood. This lack of understanding is in part due to the difficulty of studying these complicated systems with sufficient spatial and temporal resolution. However, in situ atomic force microscopy (AFM) can visualize events at low OP concentrations and with nanometer-scale resolution in a fluid cell. In the present study, we used AFM for in situ observations of organophosphate precipitation by probing glucose-6-phosphate (G6P) reacting with calcite ($10\bar{1}4$) interfaces. We chose G6P because it is a representative sugar monoester that has been detected in soils.[16,17] The mineral calcite was chosen because it is a common and well-characterized alkaline soil component with a high affinity for both inorganic and organic phosphates.[18,19] To our knowledge, there has been no in situ experimental effort to directly observe the kinetic processes of calcite dissolution in the presence of G6P and alkaline phosphatase (AP) and subsequent coprecipitation under chemical conditions that mimic soil environments. These in situ observations may improve our understanding of the mineral interface-induced organophosphate sequestration by a coupled dissolution and precipitation mechanism[20] in diverse soil systems. The aim of this study is to define the potential role of calcite ($10\bar{1}4$) interfaces in controlling organophosphate precipitation at the nanoscale.

## EXPERIMENTAL SECTION

**In Situ AFM of Calcite Dissolution.** In situ dissolution experiments were performed in a fluid cell using a Digital Instruments (Bruker) Nanoscope IIIa AFM (Multimode, operating in contact mode). A rhombohedral calcite crystal of optical quality Iceland Spar (Chihuahua, Mexico) was cleaved to expose a fresh cleavage ($10\bar{1}4$) surface. The solutions of G6P (0.1 to 5.0 mM, pH 6.1−10.2) or AP (0.2−0.8 $\mu$g/mL AP from calf intestine, 140 kDa, EIA grade, Alfa Aesar, Germany) in the absence and presence of 1.0 mM G6P at different pH values (7.0−10.0), adjusted by the addition of 0.01 M NaOH, were passed through the fluid cell containing the cleaved calcite crystal. NaCl (0.01−0.2 M at pH 8.1) and natural humic acid (HA) (0.1−0.5 mg/mL at pH 8.0, Humin, Weber, Germany) were also added to the G6P solutions to study the effects of ionic strength and an organic additive, respectively. Furthermore, the AFM experiments were carried out in the absence of buffers typically used in enzymatic studies to exclude the possibilities of buffer−calcite surface interactions. Enzyme solutions were kept at low temperatures (<0 °C) prior to use and were added to G6P solutions just before the actual start of the AFM experiments to minimize hydrolysis reactions. The experiments were conducted under constant flow, and the chosen flow rate (1 mL/min) was to ensure surface-controlled reaction rather than diffusion control.[19]

Etch-pit spreading rates during dissolution were determined (from unit-cell deep pits) for each experimental solution. The average spreading velocity of etch pits (that is, the rate of change in etch pit length along $[\bar{4}41]$ or $[48\bar{1}]$; Figure 1A,B) is given by the sum of the retreat velocity of the acute (+) and obtuse (−) steps, $v_+ + v_-$. In the presence of G6P, values of etch pit retreat rates along the $[\bar{4}2\bar{1}]$ diagonal (Figure 1D) are measured. Different locations of three different crystals per solution condition were imaged to ensure reproducibility of the results.

Ex situ dissolution experiments (1.0 mM G6P, in the absence and presence of 0.2−0.8 $\mu$g/mL AP at pH 8.1) were performed following in situ AFM experiments. The reacted calcite sample removed from the AFM fluid cell was placed in a beaker filled with ca. 10 mL of different solutions at room temperature for 24 h to observe further precipitation reactions. After 24 h, the samples were removed from the solution and quickly dried using absorbent paper and then immediately imaged in the AFM.

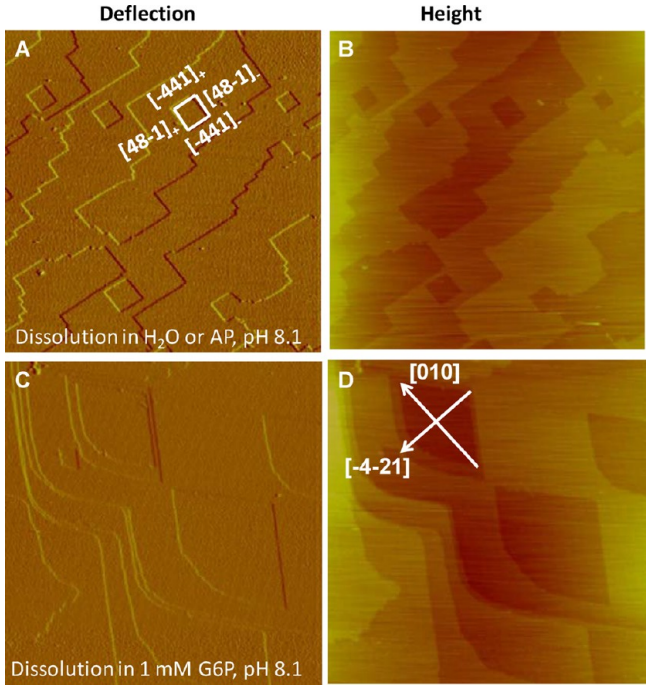


**Figure 1.** (A,C) AFM deflection and (B,D) corresponding height images illustrating calcite dissolution in water (or alkaline phosphatase, AP) at pH 8.1 (with rhombohedral etch pits bounded by $[\bar{4}41]$ and $[48\bar{1}]$) and in 1.0 mM G6P solutions at pH 8.1(with fan-shaped etch pits). The direction $[\bar{4}2\bar{1}]$ and [010] is indicated in (D). Panels A−D: 5 × 5 $\mu$m.

**X-ray Photoelectron Spectroscopy.** The use of X-ray photoelectron spectroscopy (XPS) has proven to be an ideal tool for the characterization of surface layers as well as for probing the elemental depth distribution and their bonding states; therefore, we used XPS to analyze the precipitates. Bulk reactions were carried out with the same conditions as the AFM experiments. Prior to XPS measurement as previously described,[21] all samples including standard ACP, DCPD, and HAP (Sigma-Aldrich, St. Louis, Missouri) were dried under vacuum for 8 h. Sealed tubes for all samples were used to try to minimize surface contamination prior to the XPS determinations. The samples were placed on an aluminum (Al) platform of the XPS spectrometer (VG multilab 2000 equipment ThermoVG scientific, East Grinstead, West Sussex, U.K.) and analyzed using the Al K$\alpha$ X-ray line of 1486.6 eV excitation energy at 300 W. To correct for sample charging, we used high-resolution spectra as a reference by setting the C 1s hydrocarbon peak to 284.6 eV. The background was linearly subtracted. Data analysis was performed with Thermal Advantage software (http://www.tainstruments.com). XPS experiments were repeated three times to ensure the reproducibility of results.

## RESULTS AND DISCUSSION

**Calcite Dissolution.** *a. In the Absence of AP.* Typical rhombohedral etch pits on the exposed ($10\bar{1}4$) surfaces (Figure 1A,B) were immediately formed upon dissolution in deionized


DOI: 10.1021/acs.est.5b05214
Environ. Sci. Technol. 2016, 50, 259−268

water (pH 6.1−10.2, adjusted by the addition of 0.01 M NaOH). The average spreading rate of etch pits at pH 6.1, 7.0, 8.1, 9.3, or 10.2 and was measured as 1.9 ± 0.5 ($n$ = 4), 1.8 ± 0.3 ($n$ = 5), 1.7 ± 0.3 ($n$ = 5), 1.6 ± 0.3 ($n$ = 4), and 1.5 ± 0.3 ($n$ = 4) nm/s, respectively (Figure 2A) (i.e., virtually

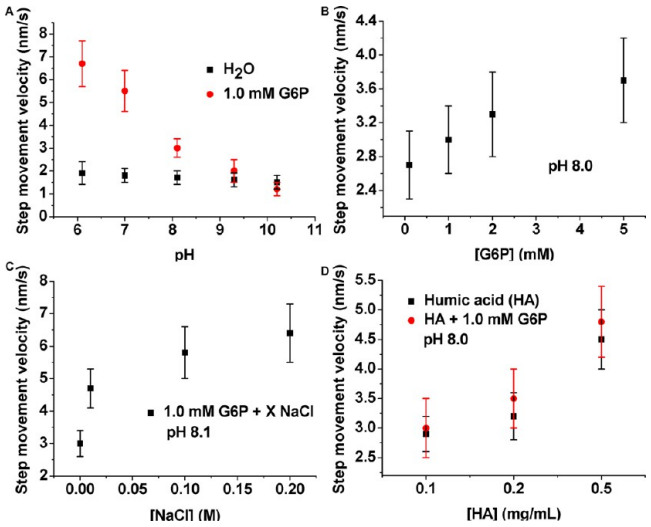


**Figure 2.** Retreat velocity of etch pits on calcite ($10\bar{1}4$) surfaces dissolved in the absence of AP at different experimental conditions. (A) pH values in the absence and presence of 1.0 mM G6P, (B) G6P concentrations at constant pH (8.0), (C) NaCl concentrations with 1.0 mM G6P at pH 8.1, and (D) HA concentrations in the absence and presence of 1.0 mM G6P at pH 8.0. In the presence of G6P, values of etch-pit retreat rates along the [$\bar{4}21$] diagonal are measured.

independent of the pH of the solution). These values are consistent with our previous results on step retreat rates.[19] In the presence of G6P, the etch pits changed from the characteristic rhombohedral morphology to fan-shaped (Figure 1C,D) as a result of the pinning of one obtuse corner. The pit retreat rate in the presence of 1.0 mM G6P at pH 6.1, 7.0, 8.1, 9.3, or 10.2 changed to 6.7 ± 1.0 ($n$ = 3), 5.5 ± 0.9 ($n$ = 3), 3.0 ± 0.4 ($n$ = 4), 2.0 ± 0.5 ($n$ = 3), or 1.2 ± 0.3 ($n$ = 3) nm/s, respectively (Figure 2A). The presence of 0.1, 1.0, 2.0, or 5.0 mM G6P at pH 8.0, increased the pit retreat rates to 2.7 ± 0.4 ($n$ = 4), 3.0 ± 0.4 ($n$ = 4), 3.3 ± 0.5 ($n$ = 4), and 3.7 ± 0.5 ($n$ = 4) nm/s, respectively (Figure 2B). When NaCl (0.01, 0.1, or 0.2 M) was introduced into 1.0 mM G6P solution (pH 8.1), the rate of pit retreat rapidly increased to 4.7 ± 0.6 ($n$ = 5), 5.8 ± 0.8 ($n$ = 4), and 6.4 ± 0.9 ($n$ = 4) nm/s, respectively (Figure 2C). The rate of pit retreat in pure humic acid solution at concentrations of 0.1, 0.2, or 0.5 mg/mL (pH 8.0) was 2.9 ± 0.3 ($n$ = 5), 3.2 ± 0.4 ($n$ = 5), or 4.5 ± 0.5 ($n$ = 5) nm/s, respectively (Figure 2D), whereas in the presence of 1.0 mM G6P (pH 8.0), the rate of pit retreat slightly increased to 3.0 ± 0.5 ($n$ = 5), 3.5 ± 0.5 ($n$ = 5), and 4.8 ± 0.6 ($n$ = 5) nm/s, respectively (Figure 2D). The change appears to be statistically insignificant after the addition of G6P into HA.

*b. In the Presence of AP.* Typical rhombohedral etch pits on the exposed ($10\bar{1}4$) surfaces dissolved in AP solutions were also present (Figure S1). The pit retreat rate in the presence of 0.2, 0.4, or 0.8 μg/mL AP alone at pH 8.1 was 1.8 ± 0.2 ($n$ = 4), 2.2 ± 0.3 ($n$ = 4), and 3.5 ± 0.5 ($n$ = 4) nm/s, respectively (Figure 3A), whereas with the addition of 1.0 mM G6P to the 0.2, 0.4, and 0.8 μg/mL AP solution (pH 8.1), the rate of pit retreat slightly decreased to 1.4 ± 0.2 ($n$ = 4), 2.1 ± 0.3 ($n$ = 4), and

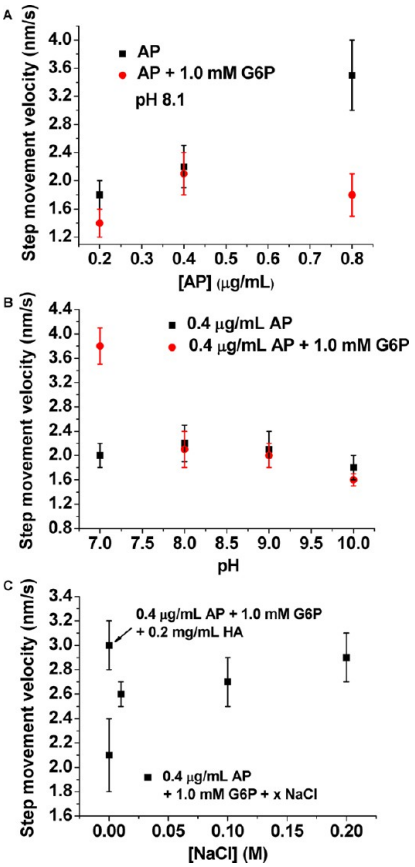


**Figure 3.** Retreat velocity of etch pits on calcite ($10\bar{1}4$) surfaces dissolved in the presence of AP at different experimental conditions. (A) AP concentrations and (B) 0.4 μg/mL AP at various pH values in the absence and presence of 1.0 mM G6P (pH 8.1), and (C) NaCl concentrations with 0.4 μg/mL AP and 1.0 mM G6P at pH 8.1.

1.8 ± 0.3 ($n$ = 4) nm/s, respectively (Figure 3A). Moreover, over a broad range of pH values between pH 7.0, 8.0, 9.0, or 10.0, the pit retreat rate in the 1.0 mM G6P solution in the presence of 0.4 μg/mL AP was 3.8 ± 0.3 ($n$ = 5), 2.1 ± 0.3 ($n$ = 5), 2.0 ± 0.2 ($n$ = 5), and 1.6 ± 0.1 ($n$ = 4) nm/s, respectively, whereas in the presence of 0.4 μg/mL AP alone, the pit retreat rate was pH-independent, remaining at about 2.0 nm/s at pH values ranging from 7 to 10 (Figure 3B). When NaCl (0.01, 0.1, or 0.2 M) was added into 1.0 mM G6P solution in the presence of 0.4 μg/mL AP (pH 8.1), the rate of pit retreat slightly increased to 2.6 ± 0.1 ($n$ = 4), 2.7 ± 0.2 ($n$ = 5), and 2.9 ± 0.2 ($n$ = 4) nm/s, respectively, compared to that without salt (2.1 ± 0.3 ($n$ = 4), pH 8.1) (Figure 3C). Also, an increase in the pit retreat rate after the addition of 0.2 mg/mL HA into 1.0 mM G6P solution in the presence of 0.4 μg/mL AP (pH 8.1) was observed (3.0 ± 0.2 ($n$ = 4)) (Figure 3C).

For calcite surfaces under far from equilibrium conditions (as is the case for our solutions), the pit retreat rates increase with decreasing pH (Figure 2A). This is consistent with our previous results under the same experimental conditions.[19] We observed that increasing the G6P or AP concentrations leads to the observed slight enhancement of etch pit spreading rates (Figure 2B). This trend is also consistent with the results from Ruiz-Agudo et al. for the case of calcite dissolution in the presence of organophosphonate compounds.[22] Moreover, it is very likely that G6P−Ca complexes form at the mineral−water interface, resulting in an increase in the dissolution rate. In the present


DOI: 10.1021/acs.est.5b05214
Environ. Sci. Technol. 2016, 50, 259−268

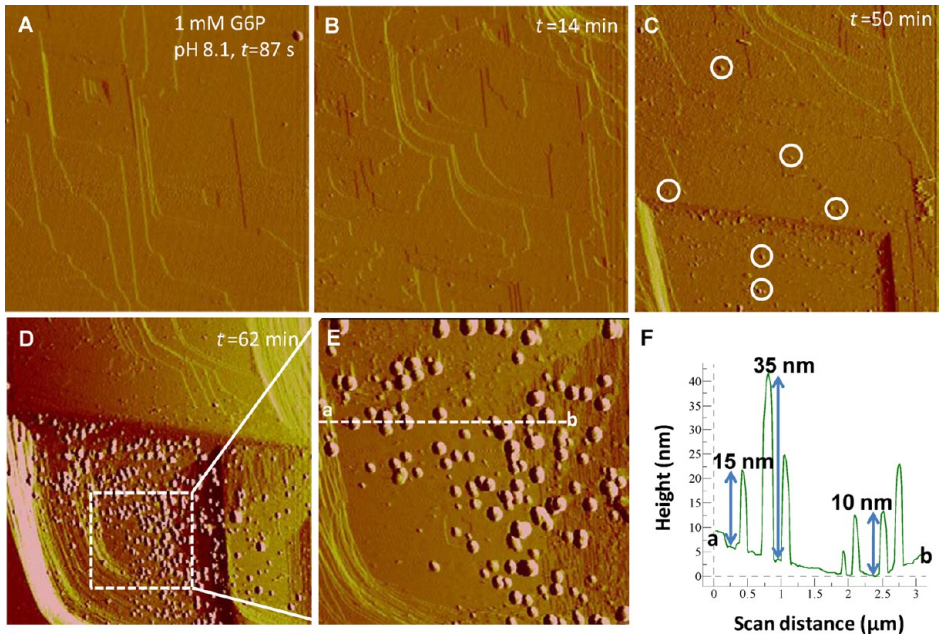


**Figure 4.** A time sequence of AFM deflection images showing (A and B) dissolution and (C–E) precipitation on the surface of calcite after exposure to a 1.0 mM G6P solution without AP at pH 8.1. After ca. 50 min of dissolution, nanoparticles formed (circled for clarity in C) and (D) subsequently grow and aggregate at the bottom of deep etch pits on the calcite $(10\bar{1}4)$ surface. (E) AFM image taken from the dotted rectangle in (D). (F) Cross-sectional analysis along the dotted line a → b in (E), showing that the height of precipitates is about 10–35 nm. Panel A, 5 × 5 $\mu$m; panels B–D, 9 × 9 $\mu$m; panel E, 3.8 × 3.8 $\mu$m.

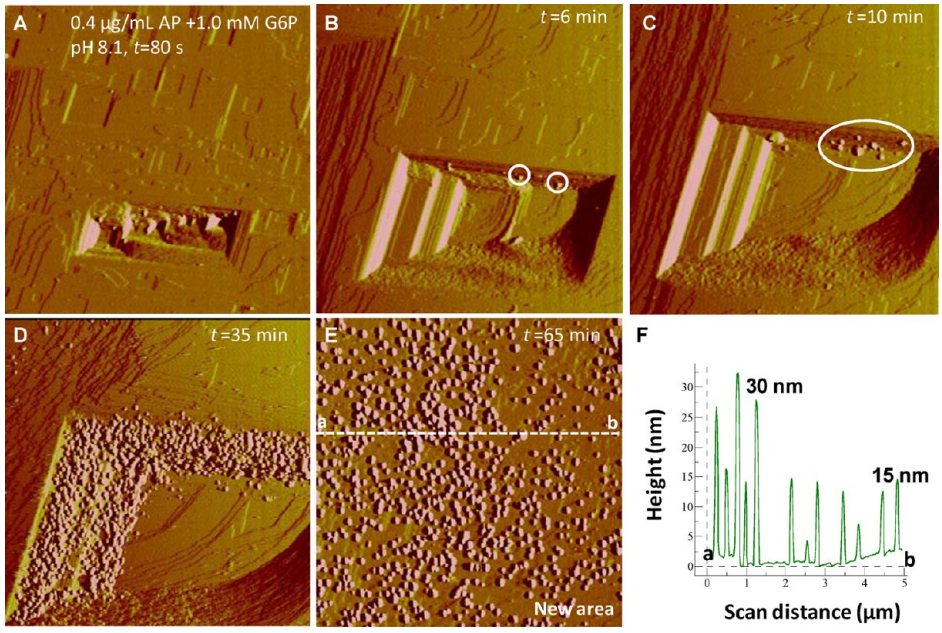


**Figure 5.** A time sequence of AFM deflection images showing (A) dissolution and (B–E) precipitation on the surface of calcite after exposure to the 1.0 mM G6P solution with 0.4 $\mu$g/mL AP at pH 8.1. After ca. 6 min of dissolution, precipitates (circled for clarity in B and C to show nanoparticles) rapidly formed along the step edges of the $[48\bar{1}]_+$ and $[\bar{4}41]-$ directions, and (D) aggregated along the $[48\bar{1}]_+$ and $[\bar{4}41]-$ step edges. (E) After 65 min of dissolution, nanoparticles formed on the whole $(10\bar{1}4)$ surface. (F) A cross-sectional analysis along a dotted line a → b in panel E showing that the height of precipitates is about 15–30 nm. Panels A–E: 5 × 5 $\mu$m.

study, however, we cannot explain how an increase in AP concentration can increase the dissolution rate (Figure 3A). In fact, the dependence of mineral dissolution rates on solution composition is complex, especially in the presence of organic additives and background electrolytes. Background electrolytes enhance the calcite dissolution rate (Figures 2C and 3C), and the extent of this enhancement seems to be determined by the ability of background ions to modify water structure dynamics as well as solute and surface hydration.[23,24] Moreover, HA, hydroxyl- and carboxylate-rich macromolecules, interact with calcite surfaces resulting in an enhancement of dissolution rate (Figure 2D), and this may arise from a decrease in the diffusive barrier by perturbations that displace water molecules.[22,25,26]



DOI: 10.1021/acs.est.5b05214
Environ. Sci. Technol. 2016, 50, 259–268

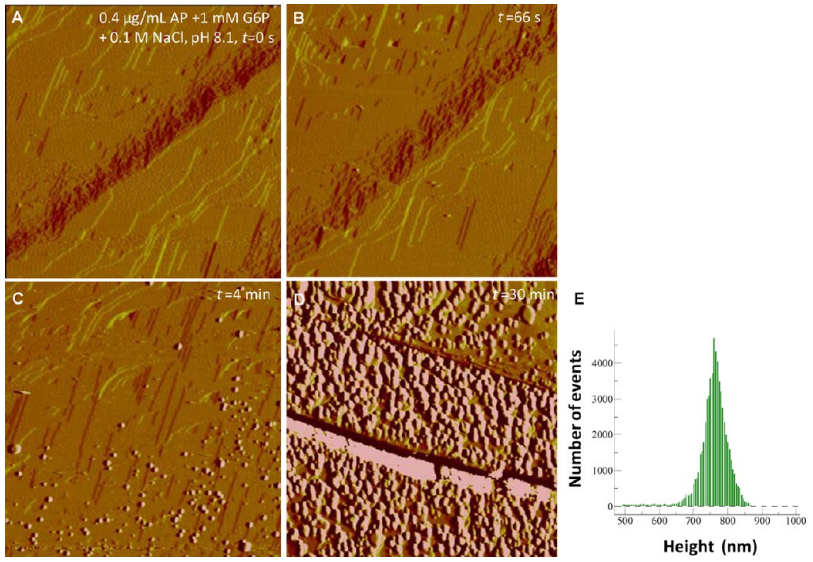


**Figure 6.** A time sequence of AFM deflection images collected at (A) $t$ = 0 s, (B) 66 s, (C) 4 min, and (D) 30 min showing salt-induced rapid precipitation on the calcite ($10\bar{1}4$) faces dissolving in solutions of 0.4 g/mL AP + 1.0 mM G6P + 0.1 M NaCl at pH 8.1. (E) Calcite substrates in (D) were covered by larger particles (about 700−800 nm in height). Panels A−D: 5 × 5 $\mu$m.

**Interfacial Precipitation on Calcite ($10\bar{1}4$) Cleavage Faces.** *a. In the Absence of AP.* The dissolving calcite substrate in the presence of 1.0 mM G6P (Figure 4A,B) provided a source of $Ca^{2+}$ ions, possibly resulting in the supersaturation of the solution at the calcite interface with respect to a G6P−Ca phase. This will drive surface-induced nucleation and growth on the calcite. At the earliest nucleation stages isolated nanoparticles (<5 nm) were formed (Figure 4C), and at subsequent growth and aggregation stages the formation of spherical particles (10−35 nm in height) (Figure 4D−F) was observed. Calcite substrates were covered by larger particles (about 50−200 nm in height) after long reaction times (1 day) (Figure S2). The size of growing particles increased when the pH was lowered to 6.1 from 8.1 at a constant concentration of 1.0 mM G6P and reaction time of 1 day (Figure S3). With increasing G6P solution concentration, when the solution pH was kept constant (pH 8.0), the etch pits changed from the characteristic rhombohedral morphology to elongated spindle shapes (Figure S4C), and faster nucleation rates were observed (Figure S4D), whereas nucleation was inhibited (Figure S5) when humic acid (HA) was added into the G6P solutions at pH 8.0 compared to that in pure G6P solution at 1.0 mM (Figure 4). As shown in Figure 2D, HA can enhance calcite dissolution; however, the addition of HA may also decrease the saturation state of precipitating G6P−Ca by forming G6P−Ca−HA organic complexes in aqueous solution. This may explain the inhibition of nucleation with increasing HA concentrations despite the expected change in calcite solubility.

For a given G6P concentration (1.0 mM, pH 8.0), faster nucleation rates were also observed with the addition of 0.2 M NaCl. After 18 min, no further growth of nucleated particles was observed (Figure S6). This could be related to the fact that the calcite surface was covered by a layer of fine precipitates that passivated the surface inhibiting the release of $Ca^{2+}$ ions into the interfacial fluid layer.

*b. In the Presence of AP.* Following 6 min of exposure to the 1.0 mM G6P solution with 0.4 $\mu$g/mL AP at pH 8.1, precipitates of nanoparticles rapidly formed along the $[48\bar{1}]_+$ and $[\bar{4}41]-$ step edges of deep etch pits (Figure 5A−C), and their aggregation and growth along such directions became evident after 35 min (Figure 5D). Upon further dissolution of the calcite substrate (65 min), nanoparticles with a height of 15−30 nm (Figure 5F) formed on the whole ($10\bar{1}4$) cleaved surface (Figure 5E). When the solution pH was changed, very few particles (at pH 7, Figure S7D−F) or even none (at pH 10, Figure S7A−C) were observed. Nevertheless, after exposing cleaved calcite surfaces to 1.0 mM G6P solution with 0.2−0.4 $\mu$g/mL AP (pH 8.1) for 1 day, the calcite surfaces were completely covered by layers of precipitates (Figure S8A,B) with a final size of about 30−50 nm (Figure S8D,E). Larger sizes of precipitates (about 100−150 nm) were observed with an increased AP concentration of 0.8 $\mu$g/mL (pH 8.1) (Figure S8C,F). Moreover, as seen by comparing Figure 5 with Figure 6, nucleation on the calcite surface is faster and larger particles (about 700−800 nm in height) nucleated (Figure 6E) after a solution of 1.0 mM G6P + 0.4 $\mu$g/mL AP with 0.1 M NaCl (pH 8.1) was injected, compared to the same solution without 0.1 M NaCl (Figure 5).

Upon input of a reaction solution of 1.0 mM G6P + 0.4 $\mu$g/mL AP in the presence of 0.2 mg/mL HA (pH 8.1), nucleation was inhibited; i.e., limited precipitation was observed on the time scale of our AFM experiments (Figure 7). In addition, a similar change in pit shape from the typical rhombohedral morphology to elongated spindle shapes was observed (Figure 7C,D).

**Identification of Precipitates on Calcite ($10\bar{1}4$) Cleavage Faces.** Following the exposure of calcite surfaces to 1.0 mM G6P solutions at pH 8.1 for 7 days, the calcite surfaces were covered by precipitated particles (Figure S9A) with an elemental composition of Ca, P, and O by SEM-EDX analyses (Figure S9B,C). The precipitates on calcite were also analyzed using FTIR and Raman spectroscopy; however, no bands apart from those corresponding to calcite were detected, possibly because the amount or thickness of the precipitates was too low to reach the detection limits of these methods.

XPS results show that a clear peak at 133.1 ± 0.1 ($n$ = 3) eV for $P_{2p}$ is observed in the calcite reacted with G6P, both in the


DOI: 10.1021/acs.est.5b05214
Environ. Sci. Technol. 2016, 50, 259−268

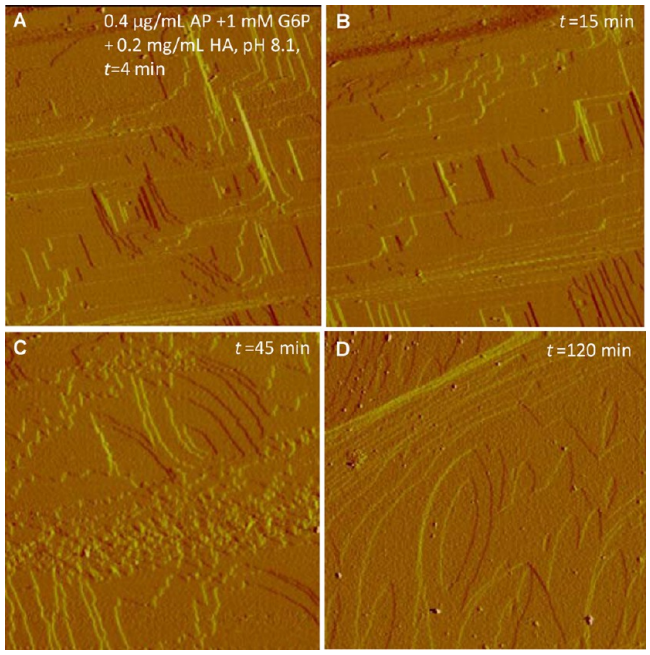


**Figure 7.** A time sequence of AFM deflection images collected at (A) $t$ = 4 min, (B) 15 min, (C) 45 min, and (D) 120 min showing the inhibition of precipitate formation in solutions of 0.4 g/mL AP + 1.0 mM G6P in the presence of 0.2 mg/mL HA at pH 8.1. Panels A–E: 5 × 5 $\mu$m.

absence and in the presence of 0.1 M NaCl, which indicates the presence of the phosphate group of the G6P rather than inorganic calcium phosphates such as amorphous calcium phosphate (ACP, 133.8 ± 0.1 eV), dicalcium phosphate dihydrate (DCPD, 134.4 ± 0.1 eV), or hydroxyapatite (HAP, 133.8 ± 0.1 eV) (Figure 8A). After introduction of 0.4 $\mu$g/mL AP at pH 8.1, the P 2p region was decomposed into three components with the same full width at half-maximum (fwhm) of 2 eV, i.e., the precipitates contain exactly three components, associated with G6P–Ca, ACP–HAP and DCPD, at 133.2 ± 0.1, 133.8 ± 0.1 and 134.4 ± 0.1 eV, respectively (Figure 8B), suggesting the presence of a mixture of organic and inorganic phosphates formed on the surface.

**Mechanisms of Interfacial Adsorption and Precipitation of G6P in the Absence of AP.** *a. Adsorption.* Using calcite surfaces, we tested the effect of various G6P concentrations and evaluated the adsorption of G6P on calcite based on the morphology changes of the growing islands (Figure S10), hillocks (Figures S12 and 13), or etch pits (Figure 1C,D), captured immediately following the injection of G6P solution into the AFM fluid cell. When G6P-bearing solutions were replaced by pure growth solutions, desorption of the G6P from the calcite surface occurred rapidly (Figure S11): the modified island and hillocks or etch pits immediately returned to their original rhombohedral morphology. Similar changes were also observed during dissolution. The adsorption–desorption reversibility suggests that G6P may not be incorporated into the calcite crystal structure under the present experimental conditions: it cannot substitute on the basis of the size of the molecule; therefore, coprecipitation with calcium and carbonate is not thermodynamically possible. Note that similar observations have been used to explain the effect of both inorganic ($HPO_4^-$, $Li^+$, and As (V)),[19,27,28] and organophosphonate (1-hydroxy ethylidene-1,1-diphosphonic acid,

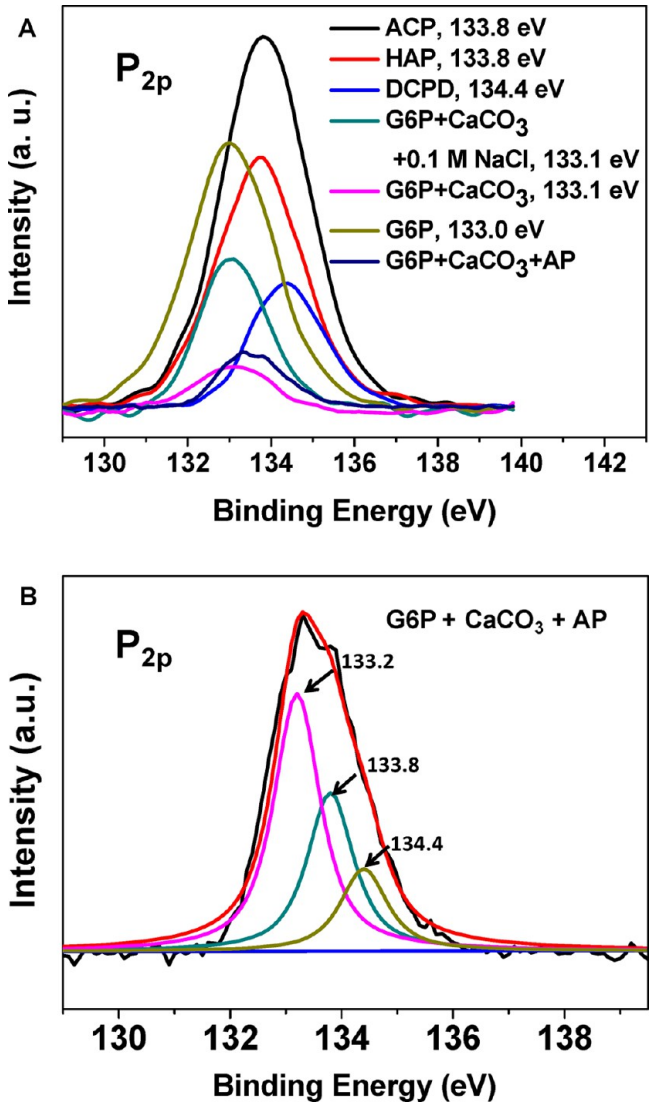


**Figure 8.** (A) High-resolution X-ray photoelectron spectra of the $P_{2p}$ region of powder calcite crystallites reacted with 1.0 mM G6P at pH 8.1 for 3 days and standard calcium phosphates including amorphous calcium phosphate (ACP), dicalcium phosphate dihydrate (DCPD), and hydroxyapatite (HAP). (B) XPS of the $P_{2p}$ region of powder calcite crystallites reacted in the presence of both 1.0 mM G6P and 0.4 $\mu$g/mL AP at pH 8.1 for 3 days.

HEDP)[22] impurities on calcite growth. Moreover, the morphology changes observed during growth and dissolution in the presence of G6P may be related to the development of islands and hillocks or etch pits with step edges parallel to $[\bar{4}\bar{2}1]$ or [010] directions (Figure 1D), corresponding to the intersection of the (0112) and (0001) faces with the cleaved surface. These two polar faces consist of alternate layers of $Ca^{2+}$ and $CO_3^{2-}$ ions in successive planes; therefore, they are unstable and unexpressed during growth or dissolution in pure solutions (Figure 1B). The adsorption of G6P to these two $[\bar{4}\bar{2}1]$ and [010] directions, may stabilize the hydration of water molecules on these faces and neutralize the dipole moment of polar faces, resulting in stabilization of the (0112) or (0001) faces. This is consistent with similar AFM observations in the presence of other additives.[27–29]

Celi and Barberis[30] have shown that the adsorption of IP occurs through their phosphate groups; properties of the


DOI: 10.1021/acs.est.5b05214
Environ. Sci. Technol. 2016, 50, 259–268

mineral (e.g., degree of crystallinity, surface porosity, specific area), available reactive adsorption sites, distance between contiguous hydroxyls, and soil solution chemistry will also influence adsorption of IP.[30] At pH 8.3, inositol hexaphosphate (IHP) can complex $Ca^{2+}$ ions even at very low concentrations by extracting $Ca^{2+}$ from the calcite surface and then favor the dissolution process of calcite.[13] Similarly, after adsorption of the G6P on calcite, complexation of the calcium ions with the phosphate ester groups of the G6P was confirmed by a shift in the P−O symmetric stretch vibration in the FTIR spectrum of the G6P in the presence of calcium ions (Figure S14). The broad band of the asymmetric stretch vibrations of P−O at 1091 $cm^{-1}$ can be coupled by the vibrations of the glucose group.[31−34]

G6P in its doubly deprotonated form ($LH_2$) is stable in a pH range of 6.0−8.0 (Figure S15) because the phosphate group can be twice deprotonated ($pK_{a1}$ = 1.0 and $pK_{a2}$ = 6.01) for G6P and similar organic monophosphate molecules.[35] The liberation of a third proton could occur in a highly alkaline solution ($pK_{a3}$ = 12.3);[36] that is, the deprotonation of the anomeric OH group of the glucose moiety.[37] According to the speciation calculations (Figure S15), various mononuclear and dinuclear species are present in our experimental system. A phosphate group coordinated in monodentate or bidentate as a bridging ligand proved to be the primary binding mode on the basis of previous NMR analyses, and no direct involvement of the alcohol−OH groups of glucose in metal binding could be hypothesized due to the unfavored steric hindrance of the organic moiety.[37] Moreover, a surface complexation model of calcite postulates the formation of the two primary hydration sites, > $CaOH^0$ and > $CO_3H^0$ (where > represents the surface site of the mineral lattice) with a 1:1 stoichiometry on the cleavage ($10\bar{1}4$) surface exposed to the aqueous solution.[38,39] Therefore, > Ca-$G6P^{2-}$ complexes may be the predominant surface species under our experimental conditions at pH 8.1. However, this needs to be confirmed after acquiring thermodynamic data on the stability of this surface complex.

*b. Precipitation.* Following adsorption of the G6P on calcite, the condensed surface complexes could finally convert to surface precipitates over a short time (<1 h) (Figure 4). Initially, the negatively charged G6P would sequester the calcium ions, thus lowering the free calcium concentration in solution at the calcite interfaces and preventing nucleation outside adsorbed G6P sites on calcite. With continued release of $Ca^{2+}$ ions during calcite dissolution, the interfacial solution eventually reaches sufficiently high supersaturation to form the G6P−Ca precipitates by a coupled dissolution-reprecipitation mechanism.[40] This adsorption−precipitation process of G6P on calcite is similar to that of IHP on amorphous aluminum hydroxide[41] and phosphate on goethite,[42] although the former needs a longer time (4 days) to form a Al−IHP precipitate at higher concentrations of IHP (2.2 mM) at ambient temperature. It is nevertheless possible that the amount of surface precipitates formed within a short reaction time is lower than the detection limit (i.e., concentration resolution) of various spectroscopy techniques, such as solid-state nuclear magnetic resonance (NMR) spectroscopy, rather than the possibility that IHP (with six phosphate groups in one IHP molecule) has a greater chelating ability to bind cations and transform to surface precipitates than other organophosphates such as G6P. The transition from sorption complexation to surface precipitation has also been reported to be related to mineral particle size[43] and crystalline phase.[44] In the present study, our results support the idea of ion binding at the mineral surface that may play a role in precipitate formation. However, another mechanism is also possible: that on the release of $Ca^{2+}$ ions from the dissolving calcite surface, precipitates form in solution and then attach to the calcite surface.[19] Local ion binding at the mineral interface can play a significant role in inducing precipitation.[45] Although the probability of nucleation scales exponentially with the free energy barrier, it also scales exponentially with a kinetic barrier related to processes such as ion desolvation and binding.[45]

Some recent results have shown that mineral surface-promoted hydrolysis of organophosphates is present, although the extent of hydrolysis is small.[32,46] However, our XPS results did not provide any evidence for the presence of orthophosphate on calcite (Figure 8A).

**Mechanisms of Interfacial Precipitation of G6P in the Presence of AP.** Enzyme-catalyzed release of glucose from G6P can occur both in solution and on calcite surfaces. The occurrence of interfacial enzymatic hydrolysis can be supported by the observed increased step retreat rates with an increase of AP concentrations (Figure 3A), suggesting rapid enzyme adsorption and subsequent hydrolysis reaction on calcite (Figure S8). Within the reaction times of our experiments, the conversion of adsorbed G6P by AP into glucose and orthophosphate was incomplete, as shown by the XPS results (Figure 8B). The interfacial hydrolysis of G6P forms two products: glucose that may be released into solution whereas orthophosphate may readsorb onto calcite, possibly having an effect on the surface charge to influence enzyme catalyzed interfacial reactions. In addition, according to the amount of precipitate formed on calcite, a slower rate of hydrolysis at pH 7.0 and 10.0 (Figure S7) compared to that at pH 8.1 (Figure 5) is deduced, demonstrating that the catalytic optimum at the mineral interface is pH-dependent. This is similar to acid phosphatase catalyzing hydrolysis of glucose-1-phosphate.[47] Increasing enzyme concentration caused a significant increase in the size for precipitates on calcite (Figure S8), indicating that the catalytic activities are also concentration-dependent. Further studies are required to understand whether or not the formation of enzyme-surface complexes and conformation changes of the three-dimensional structure following adsorption will influence the catalytic activities at the interface where the actual enzymatic hydrolysis occurs.

XPS results showed that in addition to G6P−Ca, other precipitates that may include three inorganic P components of ACP−HAP and DCPD form on calcite surfaces in the presence of AP (Figure 8). Their formation is due to the dissolution of calcite and the enzymatic hydrolysis of G6P in the presence of AP, that provide a source of $Ca^{2+}$ and orthophosphate ions, resulting in nucleation and growth of an inorganic calcium phosphate (Ca−P) phase. It has been shown that the precipitation of Ca−P phases may occur through the initial formation of various precursor phases, including ACP, DCPD, and octacalcium phosphate (OCP), prior to the transformation to the most thermodynamically stable HAP.[48] Moreover, our previous observations have demonstrated that the precipitation of HAP on calcite involves the formation and aggregation of nanosized clusters, which serve as building blocks for ACP, that subsequently transform into the final HAP phase,[49] most likely through a dissolution−recrystallization process rather than a solid-state transition.

Finally, we noticed that precipitation was inhibited as HA was present in the G6P solutions with (Figure 7) and without


DOI: 10.1021/acs.est.5b05214
Environ. Sci. Technol. 2016, 50, 259−268

AP (Figure S5). The most likely explanation is the competitive adsorption of HA, G6P, and AP. This is based on the obvious changes in etch pit shapes (Figure S5F and Figure 7D) and the increase of step retreat rates (Figures 2D and 3C), i.e., HA may exhibit a relatively stronger adsorption on calcite than G6P and AP. Moreover, AP has an isoelectric point of 4.4−5.8 and the pH optimum for its activity and stability is pH 8−10;[50] therefore, AP is net negative above pH 5.8. In the studied pH range, HA is negatively charged possibly due to the dissociation of $H^+$ from the carboxylic acid and phenolic groups in the HA macromolecules.[51,52] The dissociation of carboxylic acid groups usually occurs at pH > 3, whereas the phenolic groups undergo dissociation at pH > 9.[53] This ionization would lead to an increase of negatively charged HA molecules. Negatively charged HAs are the main organic components in soils, and the complexation between enzymes and soluble HA in soils may result in copolymerization[54] and encapsulation[55] through electrostatic and hydrophobic interactions.[56,57] This will inhibit the enzyme activities.[58,59] However, in the pH range of the present study, both HA and AP are negatively charged, and the formation of the HA−AP complexes is thermodynamically unfavorable due to electrostatic repulsion. Therefore, one potential reason for the inhibition of the precipitate formation in the presence of HA is the competitive adsorption. Another possibility is that HA could complex with aqueous calcium, thereby reducing the supersaturation with respect to G6P−Ca or Ca−P precipitation.

**Implications.** A fundamental challenge in the study of soil P dynamics is to assess the relative importance of physicochemical and biochemical processes in supplying plant-available P and predicting their fates.[60] Esters of phosphoric acid constitute a sizable fraction of the total phosphorus supply in the environment and thus play an important role in the global phosphorus cycle. In this study, direct AFM observations and kinetic analyses have been applied to observe and predict the behavior of enzymatic hydrolysis of phosphate esters on mineral surfaces to produce the orthophosphate that is often a required step preceding phosphorus uptake by plants and microorganisms.[47] We show that calcite surfaces[61,62] can efficiently concentrate enzymes to form microchemical interfacial environments via the formation of a catalytically active layer of AP, thereby enhancing the possibilities of dissolution, hydrolysis, and precipitation reactions on mineral interfaces. Our results provide dynamic insights into how organic P can be sequestered and carbon (from glucose) can be mobilized through mineral interfacial reactions in soils.

## ■ ASSOCIATED CONTENT

### Supporting Information

The Supporting Information is available free of charge on the ACS Publications website at DOI: 10.1021/acs.est.5b05214.

AFM images of calcite dissolution under different reaction conditions in the absence of AP (Figures S1−S6); AFM images of calcite dissolution in the presence of AP (Figures S7, S8); SEM image and EDX spectra of the ex situ formation of precipitates on calcite (Figure S9); AFM images of calcite growth under different reaction conditions (Figures S10−S13); FTIR spectrum of the G6P solution (Figure S14); speciation distributions of the G6P at different pH values (Figure S15). (PDF)

## ■ AUTHOR INFORMATION


### Corresponding Authors

*Phone: +86-27-87288095; e-mail: ljwang@mail.hzau.edu.cn.
* E-mail: putnisc@uni-muenster.de.


### Notes

The authors declare no competing financial interest.

## ■ ACKNOWLEDGMENTS

This work was supported by the National Natural Science Foundation of China (41471245 and 41071208), a Specialized Research Fund for the Doctoral Program of Higher Education (20130146110030), and the Fundamental Research Funds for the Central Universities (2662015PY206 and 2662015PY116). C.V.P. and A.P. acknowledge support through EU Marie Curie initial training networks (FlowTrans, $CO_2$ React, and Minsc). E.R.-A. acknowledges funding from the Spanish Government (grant MAT2012-37584) and the Junta de Andalucía (research group RNM-179 and project P11-RNM-7550-ERDF funds) as well as the receipt of a Ramón y Cajal grant from the Spanish Government (Ministerio de Economía y Competitivad).

## ■ REFERENCES


(1) Worsfold, P. J.; Monbet, P.; Tappin, A. D.; Fitzsimons, M. F.; Stiles, D. A.; McKelvie, I. D. Characterisation and quantification of organic phosphorus and organic nitrogen components in aquatic systems: A Review. *Analy. Chim. Acta* **2008**, *624*, 37−58.

(2) Baldwin, D. S. Organic phosphorus in the aquatic environment. *Environ. Chem.* **2013**, *10*, 439−454.

(3) Paul, E. A.; Clark, F. E. *Soil Microbiology and Biochemistry*, 2nd ed.; Academic Press: New York, 1996.

(4) Fuentes, B.; Jorquera, M.; Mora, M. L. Dynamics of phosphorus and phytate-utilizing bacteria during aerobic degradation of dairy cattle dung. *Chemosphere* **2009**, *74*, 325−331.

(5) Fuentes, B.; Dixon, E.; Mora, M. L.; Turner, B.; Bol, R. Dissolved phosphorus composition of grassland leachates following application of dairy−slurry size fractions. *J. Plant Nutr. Soil Sci.* **2012**, *175*, 78−85.

(6) Turner, B. L.; Papházy, M. J.; Haygarth, P. M.; McKelvie, I. D. Inositol phosphates in the environmental. *Philos. Trans. R. Soc., B* **2002**, *357*, 449−469.

(7) Luo, H.; Benner, R.; Long, R. A.; Hu, J. Subcellular localization of marine bacterial alkaline phosphatases. *Proc. Natl. Acad. Sci. U. S. A.* **2009**, *106*, 21219−23.

(8) Leprince, F.; Quiquampoix, H. Extracellular enzyme activity in soil: effect of pH and ionic strength on the interaction with montmorillonite of two acid phosphatases secreted by the ectomycorrhizal fungus Hebetomu cylindrosporum. *Eur. J. Soil Sci.* **1996**, *47*, 511−522.

(9) Giaveno, C.; Celi, L.; Richardson, A. E.; Simpson, R. J.; Barberis, E. Interaction of phytases with minerals and availability of substrate affect the hydrolysis of inositol phosphates. *Soil Biol. Biochem.* **2010**, *42*, 491−498.

(10) Baldwin, D. S.; Beattie, J. K.; Coleman, L. M.; Jones, D. R. Phosphate ester hydrolysis facilitated by mineral phases. *Environ. Sci. Technol.* **1995**, *29*, 1706−1709.

(11) Celi, L.; Presti, M. D.; Ajmore-Marsan, F.; Barberis, E. Effects of pH and electrolytes on inositol hexaphosphate interaction with goethite. *Soil Sci. Soc. Am. J.* **2001**, *65*, 753−760.

(12) Fuentes, B.; de la Luz Mora, M.; Bol, R.; Francisca San Martin, F.; Pérez, E.; Cartes, P. Sorption of inositol hexaphosphate on desert soils. *Geoderma* **2014**, *232−234*, 573−580.

(13) Celi, L.; Lamacchia, S.; Barberis, E. Interaction of inositol phosphate with calcite. *Nutr. Cycling Agroecosyst.* **2000**, *57*, 271−277.

(14) Norde, W. Adsorption of proteins from solution at the solid-liquid interface. *Adv. Colloid Interface Sci.* **1986**, *25*, 267−340.

(15) Helassa, N.; Quiquampoix, H.; Noinville, S.; Szponarski, W.; Staunton, S. Adsorption and desorption of monomeric Bt (*Bacillus*




DOI: 10.1021/acs.est.5b05214
*Environ. Sci. Technol.* 2016, 50, 259−268

*thuringiensis*) Cry1Aa toxin on montmorillonite and kaolinite. *Soil Biol. Biochem.* **2009**, *41*, 498−504.
(16) Pant, H. K.; Warman, P. R.; Nowak, J. Identification of soil organic phosphorus by P-31 nuclear magnetic resonance spectroscopy. *Commun. Soil Sci. Plant Anal.* **1999**, *30*, 757−772.
(17) Espinosa, M.; Turner, B. L.; Haygarth, P. M. Preconcentration and separation of trace phosphorus compounds in soil leachate. *J. Environ. Qual.* **1999**, *28*, 1497−1504.
(18) Suzuki, T.; Inomata, S.; Sawada, K. Adsorption of phosphate on calcite. *J. Chem. Soc., Faraday Trans. 1* **1986**, *82*, 1733−1743.
(19) Wang, L. J.; Ruiz-Agudo, E.; Putnis, C. V.; Menneken, M.; Putnis, A. Kinetics of calcium phosphate nucleation and growth on calcite: Implications for predicting the fate of dissolved phosphate species in alkaline soils. *Environ. Sci. Technol.* **2012**, *46*, 834−842.
(20) Ruiz-Agudo, E.; Putnis, C. V.; Putnis, A. Coupled dissolution and precipitation at mineral-fluid interfaces. *Chem. Geol.* **2014**, *383*, 132−146.
(21) Li, S. Y.; Wu, S. S.; Nan, D. F.; Zhang, W. J.; Wang, L. J. Inhibition of pathological mineralization of calcium phosphate by phosphorylated osteopontin peptides through step-spedific interactions. *Chem. Mater.* **2014**, *26*, 5605−5612.
(22) Ruiz-Agudo, E.; Di Tommaso, D.; Putnis, C. V.; de Leeuw, N.; Putnis, A. Interactions between organophosphonate-bearing solutions and $(10\bar{1}4)$ calcite surfaces: An atomic force microscopy and first-principles molecular dynamics study. *Cryst. Growth Des.* **2010**, *10*, 3022−3035.
(23) Ruiz-Agudo, E.; Kowacz, M.; Putnis, C. V.; Putnis, A. The role of background electrolytes on the kinetics and mechanism of calcite dissolution. *Geochim. Cosmochim. Acta* **2010**, *74*, 1256−1267.
(24) Stack, A. G. Molecular dynamics simulations of solvation and kink site formation at the {001} Barite-water interface. *J. Phys. Chem. C* **2009**, *113*, 2104−2110.
(25) Elhadj, S.; De Yoreo, J. J.; Hoyer, J. R.; Dove, P. M. Role of molecular charge and hydrophilicity in regulating the kinetics of crystal growth. *Proc. Natl. Acad. Sci. U. S. A.* **2006**, *103*, 19237−19242.
(26) Piana, S.; Jones, F.; Gale, J. D. Aspartic acid as a crystal growth catalyst. *CrystEngComm* **2007**, *9*, 1187−1191.
(27) Wang, L. J.; Ruiz-Agudo, E.; Putnis, C. V.; Putnis, A. Direct observations of the modificatioin of calcite growth morphology by $Li^+$ through selectively stabilizing an energetically unfavourable face. *CrystEngComm* **2011**, *13*, 3962−3966.
(28) Renard, F.; Putnis, C. V.; Montes-Hernandez, G.; Ruiz-Agudo, E.; Hovelmann, J.; Sarret, G. Interactions of arsenic with calcite surfaces revealed by in situ nanoscale imaging. *Geochim. Cosmochim. Acta* **2015**, *159*, 61−79.
(29) Momper, R.; Nalbach, M.; Lichtenstein, K.; Bechstein, R.; Kühnle, A. Stabilization of polar step edges on calcite (104) by the adsorption of congo red. *Langmuir* **2015**, *31*, 7283−7287.
(30) Celi, L.; Barberis, E. Abiotic stabilization of organic phosphorus in the environment. In: Turner, B. L.; Frossard, E.; Baldwin, D. S. (Eds.). *Organic Phosphorus in the Environment*. CAB International, Wallingford, UK, pp 113−132, 2005.
(31) Max, J.; Chapados, C. Glucose and fructose hydrates in aqueous solution by IR spectroscopy. *J. Phys. Chem. A* **2007**, *111*, 2679−2689.
(32) Olsson, R.; Giesler, R.; Loring, J. S.; Persson, P. Adsorption, desorption, and surface-promoted hydrolysis of glucose-1-phosphate in aqueous goethite ($\alpha$-FeOOH) suspensions. *Langmuir* **2010**, *26*, 18760−18770.
(33) Chen, J. M.; Pan, T.; Chen, X. D. Application of second derivative spectrum prepares in quantification measuring glucose-6-phosphate and fructose-6-phosphate using a FTIR/ATR method. *Optics Precision Eng.* **2006**, *14*, 1−7.
(34) Pasternya, K.; Chełmecka, E.; Wrzalik, R.; Szeja, W. Theoretical DFT study on glucose-6-phosphate. *J. Mol. Struct.* **2005**, *744*−*747*, 929−936.
(35) Atkari, K.; Kiss, T.; Bertani, R.; Martin, R. B. Interactions of aluminum (III) with phosphates. *Inorg. Chem.* **1996**, *35*, 7089−7094.
(36) Champmartin, D.; Rubini, P.; Lakatos, A.; Kiss, T. Complexes of aluminum (III) with glucose-6-phosphate in aqueous solutions. *J. Inorg. Biochem.* **2001**, *84*, 13−21.
(37) Izatt, R. M.; Rytting, J. H.; Hansen, L. D.; Christensen, J. J. Thermodynamics of proton dissociation in dilute aqueous solution. V. An entropy titration study of adenosine, pentoses, hexoses, and related compounds. *J. Am. Chem. Soc.* **1966**, *88*, 2641−2645.
(38) van Cappellen, P.; Charlet, L.; Stumm, W.; Wersin, P. A surface complexation model of the carbonate mineral-aqueous solution interface. *Geochim. Cosmochim. Acta* **1993**, *57*, 3505−3518.
(39) Pokrovsky, O. S.; Mielczarski, J. A.; Barres, O.; Schott, J. Surface speciation models of calcite and dolomite/aqueous solution interfaces and their spectroscopic evaluation. *Langmuir* **2000**, *16*, 2677−2688.
(40) Putnis, A.; Putnis, C. V. The mechanism of reequilibration of solids in the presence of a fluid phase. *J. Solid State Chem.* **2007**, *180*, 1783−1786.
(41) Yan, Y.; Li, W.; Yang, J.; Zheng, A.; Liu, F.; Feng, X.; Sparks, D. L. Mechanism of myo-hexakisphosphate sorption on amourphous aluminum hydroxide: Spectroscopic evidence for rapid surface precipitation. *Environ. Sci. Technol.* **2014**, *48*, 6735−6742.
(42) Wang, L. J.; Putnis, C. V.; Ruiz-Agudo, E.; Hövelmann, J.; Putnis, A. In situ imaging of interfacial precipitation of phosphate on goethite. *Environ. Sci. Technol.* **2015**, *49*, 4184−4192.
(43) Yan, Y.; Koopal, L. K.; Li, W.; Zheng, A.; Yang, J.; Liu, F.; Feng, X. Size-dependent sorption of myo-inositol hexakisphosphate and orthophosphate on nano-$\gamma$-$Al_2O_3$. *J. Colloid Interface Sci.* **2015**, *451*, 85−92.
(44) Müller, K.; Foerstendorf, H.; Brendler, V.; Rossberg, A.; Stolze, K.; Gröschel, A. The surface reactions of U(VI) on $\gamma$-$Al_2O_3$: In situ spectroscopic evaluation of the transition from sorption complexation to surface precipitation. *Chem. Geol.* **2013**, *357*, 75−84.
(45) Smeets, P. J.; Cho, K. R.; Kempen, R. G. E.; Sommerdijk, N. A. J. M.; De Yoreo, J. J. Calcium carbonate nucleation driven by ion binding in a biomimetic matrix revealed by in situ electron microscopy. *Nat. Mater.* **2015**, *14*, 394−399.
(46) Baldwin, D. S.; Beattie, A. K.; Coleman, L. M. Hydrolysis of an organophosphate ester by manganese dioxide. *Environ. Sci. Technol.* **2001**, *35*, 713−716.
(47) Olsson, R.; Giesler, R.; Loring, J. S.; Persson, P. Enzymatic hydrolysis of organic phosphates adsorbed on mineral surfaces. *Environ. Sci. Technol.* **2012**, *46*, 285−291.
(48) Wang, L. J.; Nancollas, G. H. Calcium orthophosphates: Crystallization and dissolution. *Chem. Rev.* **2008**, *108*, 4628−4669.
(49) Wang, L. J.; Li, S. Y.; Ruiz-Agudo, E.; Putnis, C. V.; Putnis, A. Posner's cluster revisited: Direct imaging of nucleation and growth of nanoscale calcium phosphate clusters at the calcite-water interface. *CrystEngComm* **2012**, *14*, 6252−6256.
(50) Fosset, M.; Chappelet-Tordo, D.; Lazdunski, M. Intestinal alkaline phosphatase: Physical properties and quaternary structure. *Biochemistry* **1974**, *13*, 1783−1788.
(51) Zhang, X.; Bai, R. Mechanisms and kinetics of humic acid adsorption onto chitosan-coated granules. *J. Colloid Interface Sci.* **2003**, *264*, 30−38.
(52) Alvarez-Puebla, R. A.; Garrido, J. J. Effect of pH on the aggregation of a gray humic acid in colloidal and solid states. *Chemosphere* **2005**, *59*, 659−667.
(53) Tate, K. R.; Theng, B. K. G. Organic matter and its interaction with inorganic soil constituents. In *Soils with Variable Charge, New Zealand Society Soil Science*; Theng, B. K. G., Ed.; Soils Bureau: Lower Hutt, New Zealand, 1980; pp 225−249.
(54) Rao, M. A.; Russo, F.; Granata, V.; Berisio, R.; Zagari, A.; Gianfreda, L. Fate of prions in soil: Interaction of a recombinant ovine prion protein with synthetic humic-like mineral complexes. *Soil Biol. Biochem.* **2007**, *39*, 493−504.
(55) Sarkar, J. M. Formation of [$^{14}$C]cellulase-humic complexes and their stability in soil. *Soil Biol. Biochem.* **1986**, *18*, 251−254.
(56) Tomaszewski, J. E.; Schwarzenbach, R. P.; Sander, M. Protein encapsulation by humic substances. *Environ. Sci. Technol.* **2011**, *45*, 6003−6010.


DOI: 10.1021/acs.est.5b05214
*Environ. Sci. Technol.* 2016, 50, 259−268

(57) Tan, W. F.; Koopal, L. K.; Norde, W. Interaction between humic acid and lysozyme, studied by dynamic light scattering and isothermal titration calorimetry. *Environ. Sci. Technol.* **2009**, *43*, 591−596.
(58) Ladd, J. N.; Butler, J. H. A. Inhibitory effect of soil humic compounds on the proteolytic enzyme Pronase. *Aust. J. Soil Res.* **1969**, *7*, 241−251.
(59) Li, Y.; Tan, W.; Koopal, L. K.; Wang, M. X.; Liu, F.; Norde, W. Influence of soil humic and fulvic acid on the activity and stability of lysozyme and urease. *Environ. Sci. Technol.* **2013**, *47*, 5050−5056.
(60) Bünemann, E. K. Assessment of gross and net mineralization rates of soil organic phosphorus−A review. *Soil Biol. Biochem.* **2015**, *89*, 82−98.
(61) Morse, J. W.; Arvidson, R. S.; Luttge, A. Calcium carbonate formation and dissolution. *Chem. Rev.* **2007**, *107*, 342−381.
(62) Teng, H.; Chen, Y.; Pauli, E. Direction specific interactions of 1,4-dicarboxylic acid with calcite surfaces. *J. Am. Chem. Soc.* **2006**, *128*, 14482−14484.


DOI: 10.1021/acs.est.5b05214
*Environ. Sci. Technol.* 2016, 50, 259−268